Published in final edited form as:
J Neurosci Methods. 2010 August 30; 191(2): 222–226. doi:10.1016/j.jneumeth.2010.07.001.

A facile method for immunofluorescence microscopy of highly autofluorescent human retinal sections using nanoparticles with large Stokes shifts

Howard R. Petty[1,2], **Victor M. Elner**[1,3], **Takahiro Kawaji**[1], **Andrea Clark**[1], **Debra Thompson**[1], and **Dong-Li Yang**[1]

[1]Department of Ophthalmology and Visual Sciences, University of Michigan Medical School, Ann Arbor, Michigan

[2]Department of Microbiology and Immunology, University of Michigan Medical School, Ann Arbor, Michigan

[3]Department of Pathology, University of Michigan Medical School, Ann Arbor, Michigan

Abstract

The human retina is rich in autofluorescent species, such as lipofuscin and melanin. Consequently, it is difficult to localize antigens in the human retina using immunofluorescence microscopy. To address this issue, we have developed a methodology to tag retinal antigens using quantum dot nanoparticles that absorb in the ultraviolet and emit in the infrared, thereby avoiding the visible spectrum. This protocol dramatically improves signal-to-background autofluorescence ratios of immunofluorescence images of human retinal sections, thus enhancing the specific fluorescence in microscopic studies. Of particular note is the ability to detect antigens within the brightly autofluorescent RPE cell layer.

Keywords

retina; fluorescence; nanoparticles; human

1. Introduction

The human retina contains an abundance of endogenous fluorescent components such as lipofuscin granules, melanins, carotinoids, and xanthophylls. Moreover, retinal autofluoresence, especially that of lipofuscin, accumulates over time becoming quite high among samples from older donors (Delori et al., 2001). Due to this autofluorescence in the visible spectrum, it is difficult to use conventional immunofluorescence microscopy to localize molecules within tissue sections of human retina, especially the RPE layer, as well as other pigmented ocular tissues. In general, immunolocalization within the human retina depends upon immunohistochemistry tools, such as immunoperoxidase labeling. Several groups have worked to develop alternate procedures to perform immunofluorescence microscopy on human retinal tissue sections, which focus largely on reducing the RPE component of tissue autofluorescence. For example, Sall et al. (2004) utilize 0.2% potassium permanganate to bleach pigment and reduce the autofluorescence of sections. This protocol

Address requests for reprints and correspondence to: Howard R. Petty, PhD, University of Michigan, Kellogg Eye Center, 1000 Wall Street, Ann Arbor, Michigan 48105, hpetty@umich.edu.

is reported to reduce the contribution of melanins to the images, presumably by chemically altering autofluorescent compounds. A second approach to reduce retinal autofluorescence is to stain sections with 1% Sudan black B (Mullins et al., 2007), which presumably quenches some endogenous fluorescent species. Schnell et al. (1999) have reported that 1–10 mM CuSO4 reduces lipofuscin fluorescence of the retina. Other strategies to reduce autofluorescence include incubating sections in light boxes to photobleach potentially interfering fluorescent species prior to labeling, chemical extraction using ammonia-ethanol solutions to remove fluorescence species, and reduction of Schiff's bases formed by aldehyde fixation (for a review see Petty (2007)). Broadly, these approaches are not widely used because they do not work well, for example, due to chemical damage to the antigens in the specimen.

As chemical modification of tissue sections has not yet provided a broadly useful solution to the autofluorescence problem of human retinal sections, we have sought a physical solution to the problem. One physical characteristic of fluorescent compounds is the Stokes shift, which is the difference between the absorption and emission wavelengths of the fluorescent label. As a rule, organic dyes have Stokes shifts of ~30 to 60 nm, which is also true for autofluorescent compounds of the retina. To distinguish retinal autofluorescence from that of specific labels, it would be far better to use labels with excitation and emission wavelengths distinct from endogenous fluorescent species. For example, by using a label with a large Stokes shift, endogenous fluorescent compounds of the retina would have no infrared emission intensity when ultraviolet excitation is used. Several inorganic ions and crystals (rare-earth lanthanides and quantum dots (Qdots)) exhibit fluorescence characterized by very large Stokes shifts (~400 nm). Qdots are inorganic semiconductor nanocrystals composed of CdSe, CdS, and other compounds that possess exceptional fluorescence characteristics (Petty, 2007; Gao et al., 2005; Michalet et al., 2005), including very large Stokes shifts. By using Qdots emitting in the near infrared, the emission intensities of endogenous autofluorescent retinal compounds excited at the Qdot's ultraviolet excitation (415nm) will be virtually undetectable. In the present study we show that Qdots emitting at 800nm dramatically reduce the contribution of endogenous retinal fluorescence in immunofluorescence microscopy studies of human retinal tissue sections.

2. Materials and Methods

2.1 Materials

Phosphate-buffered saline (PBS) and endogenous biotin blocking kit were purchased from Invitrogen (Carlsbad, CA). Costar 96-well black clear-bottom plates were purchased from Fisher Scientific (Pittsburgh, PA). All other reagents were purchased from Sigma-Aldrich (St Louis, MO).

2.2 Clinical Samples

We investigated 7 human eyes obtained from 7 Caucasian subjects: 5 eyes were enucleated at our hospital due to orbital tumor and 2 healthy donor eyes were obtained from Illinois Eye Bank (Chicago, IL). All eyes were fixed immediately after an enucleation. The postmortem times preceding fixation of Eye Bank samples were 8.5 hr and 10 hr. Eyes were embedded in paraffin after overnight incubation in 4% paraformaldehyde. The mean age of patients was 67 years (range, 59 – 75 years). The use of human material was in accordance with the Declaration of Helsinki on the use of human material for scientific research.

2.3 Antibody Reagents

The following primary antibodies were used in this study: mouse monoclonal anti-RPE65 (mAb8B11; 2 μg/ml), mouse monoclonal anti-β-actin (1:2000; Sigma-Aldrich), rabbit

polyclonal anti-neuronal specific enolase (1:20; Calbiochem, San Diego, CA), mouse monoclonal anti-glyceraldehyde-3-phosphate dehydrogenase (GAPDH) (1:50; Chemicon International, Temecula, CA), and mouse IgG1 isotype control (Sigma-Aldrich). In addition to the primary antibodies listed above, the following reagents were also used in immunohistochemistry: biotin-XX conjugated goat anti-mouse IgG (1:100), biotin-XX conjugated goat anti-rabbit IgG (1:100), and Qdot800 streptavidin conjugate (1:50) were obtained from Invitrogen.

2.4 Immunohistochemistry

Paraffin-embedded normal human retinal tissue samples were prepared according to standard histochemical procedures (Elner et al., 2003) for analysis by immunostaining and fluorescence microscopy. Paraffin-embedded tissues were cut into 6 μm-thick sections. Prior to labeling, sections were deparaffinized and gradually rehydrated by sequential incubations in 100%, 95%, 80%, and 70% ethanol. After rehydration with PBS, sections were subjected to heat-mediated antigen retrieval in 10 mM citric acid buffer, pH 6.0 for 10 min. Sections were first blocked with Component A and Component B for 30 min each using Invitrogen's Endogenous Biotin Blocking kit, and then blocked with blocking solution (10% normal goat serum/6% BSA in PBS) for 1 hr at room temperature. After blocking procedures, sections were incubated with primary antibodies in 1% BSA in PBS overnight at 4°C. The sections were washed 3 times for 5 minutes each with PBS and then incubated with appropriate secondary antibodies diluted in 1% BSA in PBS for 2 hr at room temperature. After incubation, the sections were washed 3 times for 5 minutes each washed with PBS. Finally, the sections were incubated with Qdot800 streptavidin conjugate for 1.5 hr at room temperature, washed 3 times for 5 minutes each with PBS, mounted with 90% glycerol in PBS and covered with a glass coverslip.

2.5 Fluorescence microscopy

Fluorescence microscopy was performed using a 20x objective (NA=0.4) (Carl Zeiss, Inc., New York, NY) and an Andor iXon EMCCD (electron multiplying charge coupled device) camera (Andor Technology, Belfast, Northern Ireland) with a 100-Watt mercury lamp. For line profile analysis experiments, a 32x (NA=0.4) objective was used to focus on the RPE cell layer. Qdots were imaged using a 415WB100 excitation filter, a 475nm dichroic mirror, and an 800WB80 emission filter. All filters were obtained from Chroma Technology Corp. (Bellows Falls, VT). Sixteen bit deep images were collected (1Mz) with a 1.7 msec/pixel shift speed. The EMCCD chip was maintained at −90°C. Images were captured and processed with Metamorph 7.1 software (Molecular Devices, Downingtown, PA).

3. Results

We hypothesized that the contribution of retinal autofluorescence to immunofluorescence micrographs can be dramatically reduced by using fluorescent labels possessing large Stokes shifts. To test this hypothesis, we employed Qdot800 nanoparticles that absorb in the ultraviolet and emit in the near infrared. For imaging experiments, an excitation wavelength of 415 nm and an emission wavelength of 800 nm were employed. Hence, these particles exhibit a Stokes shift of roughly 400nm.

Unlabeled tissue sections of a human retina were studied. Fig. 1 shows an example of retinal autofluorescence collected with conventional filters used to detect fluorescein emission. As the retina often artificially separates from the RPE layer during routine processing, the autofluorescence of the RPE and neural retinal layers are shown separately in Fig. 1B and D, respectively. Fig. 1B is an example of the autofluorescence of the RPE and choroid layers. Fig. 1D shows the autofluorescence of the neural retina. As this figure illustrates, RPE cells

exhibit very bright autofluorescence, whereas there is less autofluorescence of the photoreceptor layer.

We next labeled tissue sections with non-specific IgG or with specific antibodies to test the ability of Qdot800 to discriminate non-specific and specific fluorescence. In the first series of experiments, sections were incubated with non-specific IgG, washed, and then incubated with a biotin-conjugated second-step anti-IgG antibody followed by streptavidin-conjugated Qdot800. Labeled sections with non-specific IgG displayed bright endogenous autofluorescence (Fig. 2A) using conventional fluorescence microscopy. However, an identical section (Fig. 2B) displayed little autofluorescence when imaged using a Qdot800 filter set (very large Stokes shift). Simply put, there is very little within these samples that absorbs at 415 nm and emits at 800 nm. In the next series of experiments, sections were stained with an antibody directed against the protein RPE65, which is expressed exclusively by RPE cells. We selected RPE65 because it is difficult to study with conventional immunofluorescence due to RPE autofluorescence. Cells were labeled with anti-RPE65 and biotin-conjugated second-step anti-IgG followed by streptavidin-Qdot800. When tissue sections labeled with anti-RPE65 and stained with Qdot800 were evaluated, bright cytoplasmic fluorescence was observed in RPE cells (Fig. 2C). Control experiments were performed in an identical fashion except that non-specific IgG was used in place of the anti-RPE65 reagent; no labeling was observed in these experiments (data not shown). RPE65 labeling (Fig. 2C) was not as punctate as sample's autofluorescence (Fig. 2A). As these results were not obtained using Qdot800 labels with a conventional filter set (data not shown), the findings cannot be due to some non-specific artifact of the filters. Six additional eyes from different patients demonstrated the same degree of lack of endogenous autofluorescence with ultraviolet excitation and infrared emission. Hence, it is possible to separate a sample's autofluorescence from the label's fluorescence.

We next used line profile analysis software to quantify the fluorescence intensities of tissue sections. Fig. 2D, trace 1, shows a line profile analysis of the autofluorescence of an unlabeled retinal section measured using a TRITC filter set. In contrast, when an unlabeled sample was viewed at the 800nm Qdot emission wavelength, only very weak fluorescence was observed (Fig. 2D, trace 3). However, when a Qdot800-labeled sample was observed, an intermediate level of specific fluorescence due to the Qdot800 label was found (Fig. 2D, trace 2). In comparing the TRITC labeled and Q-dot labeled samples, a signal-to-utofluorescent background ratio of ~50:1 was found. Thus, this imaging approach is comparable to conventional fluorescence microscopy studies, which typically exhibit signal-to-noise ratios of 10:1 to 100:1 (e.g., Benson et al., 1985).

To test an antigen distributed in other regions of the retina, we stained sections with an anti-β-actin antibody (Fig. 3). Some separation between the RPE and photoreceptor layers occurred, accounting for the gap between the layers in Fig. 3. The RPE and choroid layers are shown near the lower portion of the figure whereas the neurosensory retina is shown near the top. The intense endogenous autofluorescence of this section (Fig. 3B) was indistinguishable from that shown in Figs. 1 and 2. Although the neurosensory retina was not stained by anti-RPE65 (data not shown), it was labeled with the anti-β-actin reagent as was the RPE layer. Again, immunofluorescence localization was not masked by endogenous autofluorescence. It should be noted that the fluorescence patterns and intensities observed for background autofluorescence and Qdot800 imaging of β-actin are dramatically different, further supporting the ability of the large Stokes shift approach to separate these two kinds of fluorescence.

We also tested the antigens enolase and GAPDH, which were found in both the neural retina and RPE layers. As the neural retina also exhibits some degree of autofluorescence at

multiple wavelengths (Fig. 1), this approach is also useful for this area of the retina. Our data provide evidence that: 1) multiple antigens can be studied using this methodology, 2) multiple layers of the retina can be examined, and 3) antigens expressed at various levels can be detected.

4. Discussion

Aged human eyes exhibit very high levels of autofluorescence – unlike the eyes of many young laboratory animals used in ophthalmology research. As the study of human retinal sections is generally limited to immunohistochemisty, there is a great need for high-contrast fluorescence techniques that effectively image human retinal tissue despite its autofluorescence. In the present study, we have shown that labeling human retinal sections with infrared-emitting quantum dots enables a high level of discrimination between specific fluorescence and endogenous retinal autofluorescence. The approach relies upon avoiding the visible spectrum by exciting in the ultraviolet and detecting emission in the infrared by using a label with a very large Stokes shift. A disadvantage of the approach is that it impossible to view the fluorescence using oculars as all samples must be viewed using a sensitive camera with infrared capability. However, this approach has many advantages such as much higher contrast over conventional immunohistochemical methods.

As illustrated by the above data, eye research will greatly benefit of this approach. Although studies of all retinal layers will be improved by these methods, the greatest benefits will be seen in the RPE and related diseases such as AMD, due to the RPE cells' high levels of autofluorescence, and in the study of human retinal diseases such as proliferative vitreo-retinopathy and retinitis pigmentosa in which pigmented cells may be found diffusely throughout the affected tissue. The imaging protocol described above may also contribute to other areas of neuroscience, specifically tissues that express neuronal lipofuscin. Lipofuscin is a component of glial cells and neurons, including spiral ganglia of the auditory pathway, hippocampus, neocortex, thoracic spinal cord and others (e.g., Boellaard et al., 2004; Igarashi and Ishii, 1990).

Although the present Qdot800 strategy is an improvement over previous methods, it is limited by the background non-specific autofluorescence observed, as quantified in Fig. 3D (trace 3). Low abundance proteins distributed uniformly within cells will be difficult to observe if their intensity is near to that of the background at 800nm. However, further improvements in detection sensitivity may be realized.

Although infrared microscopy was frequently employed until the 1950's (Puchtler et al., 1980), it fell into disfavor for several decades. However, near-infrared fluorescence has many advantages, such as reduced phototoxicity and a reduction in background fluorescence. Due to its advantage of suppressing sample autofluorescence, infrared microscopy is likely to become an important methodology in immunofluorescence microscopy of tissues exhibiting high levels of autofluorescence. One improvement over the current methodology would be the use of larger Qdots, which would emit further into the infrared, thereby further suppressing autofluorescence. Another potential improvement is the use of nanoparticles that excite and emit in the infrared, thereby depriving autofluorescent retinal molecules of excitation. The latter approach will depend upon the availability of high sensitivity cameras operating in the near infrared. Additionally, it may be possible to use tandem fluorophores, in which the Stokes shifts are additive, to yield large Stokes shifts for imaging. Finally, it may be possible to develop improved imaging methods using more recently developed nanoparticles.

Acknowledgments

This work was funded by the Midwest Eye Bank. We also acknowledge the Core Center for Vision Research grant P30 EY007003.

References

Boellaard JW, Schlote W, Hofer W. Species-specific ultrastructure of neuronal lipofuscin in hippocampus and neocortex of subhuman mammals and humans. Ultrastruct Pathol. 2004; 28:341–351. [PubMed: 15764582]

Benson DM, Bryan J, Plant AL, Botto AM, Smith LC. Digital imaging fluorescence microscopy: Spatial heterogeneity of photobleaching rate constants in individual cells. J Cell Biol. 1885; 100:1309–1323. [PubMed: 3920227]

Delori FC, Goger DG, Dorey CK. Age-related accumulation and spatial distribution of lipofuscin in RPE of normal subjects. Invest Ophthalmol Vis Sci. 2001; 42:1855–1866. [PubMed: 11431454]

Elner VM, Elner SG, Bian ZM, Kindezelskii AL, Yoshida A, Petty HR. RPE CD14 immunohistochemical, genetic, and functional expression. Exp Eye Res. 2003; 76:321–331. [PubMed: 12573661]

Gao X, Yang L, Petros JA, Marshall FF, Simons JW, Nie S. In vivo molecular and cellular imaging with quantum dots. Curr Opin Biotech. 2005; 16:63–72. [PubMed: 15722017]

Igarashi Y, Ishii T. Lipofuscin pigments in the spiral ganglion of the rat. Eur Arch Otorhinolaryngol. 1990; 247:189–193. [PubMed: 2350511]

Michalet X, Pinaud FF, Bentolila LA, Tsay JM, Doose S, Li JJ, Sundaresan G, Wu AM, Gambhir SS, Weiss S. Quantum dots for live cells, in vivo imaging, and diagnostic. Science. 2005; 307:538–544. [PubMed: 15681376]

Mullins RF, Kuehn MH, Faidley EA, Syed NA, Stone EM. Differential macular and peripheral expression of bestrophin in human eyes and its implication for best disease. Invest Ophthalmol Vis Sci. 2007; 48:3372–3380. [PubMed: 17591911]

Petty HR. Fluorescence microscopy, Emerging methods and strategies to extract weak signals with applications in immunology. Micros Res Tech. 2007; 70:687–670.

Puchtler H, Meloan SN, Paschal LD. Infrared fluorescence microscopy of stained tissues: principles and technic. Histochemistry. 1980; 68:211–230. [PubMed: 7462002]

Sall JW, Klisovic DD, O'Dorisio MS, Katz SE. Somatostatin inhibits IGF-1 mediated induction of VEGF in human retinal pigment epithelial cells. Exp. Eye Res. 2004; 79:465–476. [PubMed: 15381031]

Schnell SA, Staines WA, Wessendorf MW. Reduction of lipofuscin-like autofluorescence in fluorescently labeled tissue. J. Histochem. Cytochem. 1999; 47:719–730. [PubMed: 10330448]

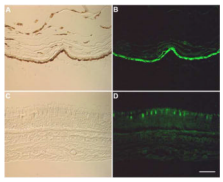

Fig. 1.

Micrographs of unstained human retina. The sample separated at the RPE-photoreceptor interface during preparation. In panels A and C differential interference contrast images are shown. Autofluorescence images are shown in panels B and D. Panels A and B show the RPE and choroid (note the pigment in panel A) whereas C and D show the neural retina. Although all retinal layers exhibit autofluorescence, RPE cells display bright autofluorescence under conditions used for conventional immunofluorescence using FITC labels (excitation filter, 475nm; emission filter, 530nm). RPE, retinal pigment epithelium; PR, photoreceptor layer; ONL, outer nuclear layer; OPL, outer plexiform layer; INL, inner nuclear layer; IPL, inner plexiform layer; GCL, ganglion cell layer. (Bar=50 μm)

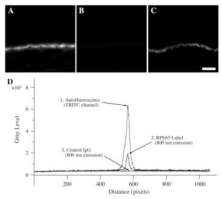

Fig. 2.

Immunofluorescence microscopy studies of human RPE/choroid sections. Panels A–C. Panels A and B show cells treated with control IgG and biotin-conjugated second-step anti-IgG followed by streptavidin-Qdot800. Panel C shows another section labeled with anti-RPE65 and biotin-conjugated second-step anti-IgG followed by streptavidin-Qdot800. In panels B and C, tissue sections were imaged using a Qdot800 filter set. In panel A, a TRITC filter set was employed. When tissue samples were examined using TRITC filters, bright autofluorescence was observed (A), as expected. Using a Qdot800 filter set the control section showed little fluorescence (B). In contrast, anti-RPE65 labeled samples demonstrated bright fluorescence localized to regions of the RPE layer (C). Unprocessed micrographs are shown. Instrument settings were identical in all of these frames to allow direct comparisons. Fluorescence micrographs were collected with camera settings of 225 EM gain, 2.4x pre-amplifier gain, and 3.0 sec. exposure. (Bar=20 m)

Panel D. Line profile analyses of images were performed to quantitatively compare fluorescence intensities of RPE layers. The intensity (grayscale) is plotted at the ordinate and position is plotted on the abscissa. The upper curve (trace 1) is the autofluorescence of unlabeled sections observed using a TRITC filter set. The lower curve is a control sample observed with the Qdot800 filter set (trace 3). The middle curve is an anti-RPE65 labeled sample (trace 2). The large Stokes shift of the Qdot800 label enables visualization at a high signal-to-noise ratio at 800 nm. The suppression of autofluorescence was noted in tissue samples from 7 patients (67 ± 7).

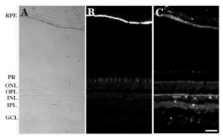

Fig. 3.

Survey micrographs of a human retina are shown. In panel A, a bright field micrograph shows the position of the RPE and neurosensory layers of the retina. Panel B shows endogenous autofluorescence observed using a TRITC filter set. On the right side, panel C shows a sample stained with an anti-β-actin antibody using a Qdot800 filter set. Note that the pattern and intensity of specific actin staining (panel C) is dramatically different than that of autofluorescence observed in panel B. (In panel A, an exposure time of 0.4 sec. was used without EM gain or pre-amplifier gain. In panels B and C, an exposure time of 1.0–3.0 sec., an EM gain of 225, and a pre-amplifier gain of 2.4x were used.) RPE, retinal pigment epithelium; PR, photoreceptor layer; ONL, outer nuclear layer; OPL, outer plexiform layer; INL, inner nuclear layer; IPL, inner plexiform layer; GCL, ganglion cell layer. (Bar = 50 μm)